Figure 3. Raman spectrum 1:1 mixture, as given in A, Figure 2, in acidic solution. Experimental conditions: 406.7-nm Kr^+ excitation; laser power, 100 mW; sensitivity, 1 μA; spectral slit width, 8 cm^{-1}; time constant, 4.4 s; scan speed, 0.75 cm^{-1}/s.

however, the intense band at 1521-cm^{-1} that was detected with 514.5-nm irradiation was not present. This suggests that the two excited states that are associated with absorption band maxima at 375 and 540 nm differ in the region of the nicotinamide group from which they originate and/or in the symmetry of their respective states, hence, giving rise to electronic transitions with different polarizations. Differences in vibronic coupling would, therefore, be evident as differences in the relative intensities of resonance Raman bands with excitation into the 375- and 540-nm electonic absorption bands. The presence of amide I and nicotinamide ring stretching Raman bands, in resonance with the 375-nm electronic transition of the blue complex, shows that extensive electronic delocalization of amide and nicotinamide ring charge exists as previously indicated.[11,12] For both amide I at 1690 cm^{-1} and $\nu(C\dot{-}\dot{-}C) + \nu(C\dot{-}\dot{-}N)$ at 1490 cm^{-1} to be resonance intensified, the electronic excited state should involve greater perturbation of bond distances and force constants represented in the resonance form

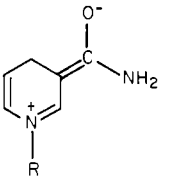

relative to the ground electronic state parameters.

Work with other carbonyl compounds has shown that a carbonyl stretching Raman band is in resonance with an electronic absorption band, if this is due to a $\pi \rightarrow \pi^*$ transition of a conjugated double-bond system and if the C=O bond in question is involved in that conjugated double-bond system.[20] Excitation into the 340-nm absorption band of NADH was found to cause enhancement of the amide I mode at 1690 cm^{-1}, suggesting that the carbonyl group is conjugated to the ring. However, in contrast to excitation into the 375-nm band of the blue Fe^{III}NADH complex, the electronic excited state of NADH should therefore involve a large perturbation of bond distances and force constants represented by the resonance form

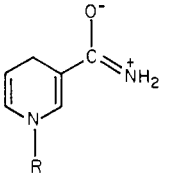

relative to the ground-state parameters.

Acknowledgment. This work was supported by part of an NIH Biomedical Research Support Grant (No. RR07105-04) to Clarkson College. We thank Dr. Paul Carey of the National Research Council of Canada for use of the Raman spectrometers.

(20) Nishimura, Y.; Tsuboi, M. *Science (Washington, D.C.)* **1980**, *210*, 1358.

State of Manganese in the Photosynthetic Apparatus. 1. Extended X-ray Absorption Fine Structure Studies on Chloroplasts and Di-μ-oxo-Bridged Dimanganese Model Compounds

J. A. Kirby, A. S. Robertson, J. P. Smith, A. C. Thompson, S. R. Cooper, and M. P. Klein*

Contribution from the Laboratory of Chemical Biodynamics, Lawrence Berkeley Laboratory, University of California, Berkeley, California 94720. *Received December 1, 1980*

Abstract: Extended X-ray absorption fine structure studies on the manganese contained in spinach chloroplasts and on certain di-μ-oxo-bridged manganese dimers of the form $(X_2Mn)O_2(MnX_2)$ (X = 2,2′-bipyridine and 1,10-phenanthroline) are reported. From these studies, the manganese associated with photosynthetic oxygen evolution is suggested to occur as a bridged transition-metal dimer with most likely another manganese. Extensive details on the analysis are included.

Since the original observation in 1937 by Pirson[1] of an absolute requirement in photosynthesis for the trace element manganese, the specific role that Mn plays has been a subject of extensive research. The general consensus is that the Mn is directly involved in photosynthetic oxygen evolution either at the active site or as a critical component of the electron-transport chain (see review by Radmer and Cheniae[2] for further details). Until now all

(1) Pirson, A. *Z. Bot.* **1937**, *31*, 193–267.

(2) Radmer, R.; Cheniae, G. In "Topics in Photosynthesis", Vol. 2; Barber, J., Ed.; Elsevier: Amsterdam, 1977; pp 303–348.

0002-7863/81/1503-5529$01.25/0

observations which have been made concerning the activity of the chloroplast-bound Mn have been by indirect methods such as NMR water proton relaxation experiments[3] and Mn release experiments using some chemical[4] or physical[5] treatments. The experimental work reported in this paper and its companion[6] is the first direct observation of the Mn contained in chloroplasts. The technique used was X-ray absorption spectroscopy (XAS) utilizing the tunable X-ray sources at the Stanford Synchrotron Radiation Laboratory (SSRL), Stanford, CA.

Two types of information can be obtained from XAS. The first is an estimate of the formal oxidation state of the element of interest, using X-ray absorption edge spectroscopy. Such studies on the Mn in chloroplasts are reported in the accompanying paper.[6] The other information allows the determination of the local structure around the atom whose XAS spectrum is being obtained. This type of experiment utilizes the postabsorption edge modulations of the photoelectron cross section which is known as extended X-ray absorption fine structure (EXAFS). The theoretical basis of the effect has been well established by Stern and Ashley and Donaich in ref 7 and 8, respectively. Analysis of the modulation patterns yield the radial distances to the neighboring atoms. To some extent the backscattering probabilities can be used for elemental identification of the ligating atoms.[9,10]

It has been known for many years that there are at least two different classes of Mn in chloroplasts. The larger fraction, the "loosely bound pool", is known to be essential for O_2 evolution. This "loosely bound pool" represents approximately two-thirds of the total Mn, and the release from its normal site into an aqueous phase can be accomplished by physical and chemical methods.[2] For differentiation between these two classes of Mn, X-ray spectra were collected on chloroplasts capable of oxygen production ("active" chloroplasts) and on chloroplasts which had the "loosely bound pool" of Mn completely removed and thus were incapable of oxygen evolution ("inactive" chloroplasts).

Materials and Methods

The preparation of various chloroplast samples is detailed in the companion paper[6,23] and will not be repeated here. The two samples used were an "active" broken chloroplast pellet and an "inactive" chloroplast pellet which had the "loosely bound pool" of Mn removed by treatment with Tris buffer (Tris = alkaline tris(hydroxymethyl)aminomethane) followed by osmotic shock. Complete removal of all aqueous Mn^{2+} was monitored by measurements of the Mn^{2+} EPR signal.

A number of model compounds were prepared or purchased for comparison with the chloroplast samples. The three reported here, di-μ-oxo-tetrakis(2,2'-bipyridine)dimanganese(III,IV) perchlorate, Mn(3,4)-bpy, di-μ-oxo-tetrakis(1,10-phenanthroline)dimanganese(III,IV) perchlorate, Mn(3,4)phen, and di-μ-oxo-tetrakis(1,10-phenanthroline)dimanganese(IV,IV) perchlorate Mn(4,4)phen, were prepared and characterized by literature methods.[11,12,13] The powdered crystalline samples were mixed with a binding agent of powdered cellulose and pressed into 1.25-in. diameter pellets in sufficient quantities so that approximately 90% of the incident X-ray flux was absorbed in the sample when the X-ray energy was just higher than the Mn K or 1s absorption edge.

Experimental Section

The X-ray absorption spectra were obtained at the Standford Synchrotron Radiation Laboratory (SSRL). The model compound data were collected in the standard absorption mode, described elsewhere.[14] Due to the very low concentration of Mn in the chloroplast samples (of the order of 100 μM) and the large background absorption by the rest of the sample (e.g., water, protein, and phospholipid), it was not possible to collect usable absorption data in a reasonable period of time. The chloroplasts spectra instead were collected in the fluorescent detection mode where the relative X-ray absorbance was obtained by measuring the excitation function of X-ray fluorescence characteristic of Mn.[15] The X-ray detector used was a triplet Si(Li) solid-state detector built by the Nuclear Instrument and Methods Group at Lawrence Berkeley Laboratory.[16] Even with the sensitivity enhancement provided by the fluorescent EXAFS technique,[15] it was still necessary to use the focused X-ray line[17] at SSRL to obtain as intense an incident X-ray flux as possible. The "active" chloroplast spectra were obtained in approximately 24 h on a focused line. The inactive chloroplast spectra were obtained in approximately the same amount of beam time 2 weeks later. The large number of individual spectra were eventually coadded to produce one data analysis spectrum for each sample.

General Data Analysis Method. EXAFS data processing is described in detail elsewhere[18] and thus will be only briefly outlined here.

The first step was to condense the numerous individual spectra that were collected on each sample into one final coadded spectrum. A significant problem at this step was to maintain an energy reference for each spectrum relative to a preselected standard. For the chloroplast spectra this presented some problems, which are addressed later. The data are then expressed as a relative EXAFS modulation, generally defined by[7,8]

$$\chi(k) = [\mu(k) - \mu_{BG}(k)]/\mu_0(k) \quad (1)$$

where χ is the fine structure modulation (EXAFS), μ is the observed X-ray absorption cross section, μ_0 is the photoelectric cross section for the free atom, and μ_{BG} is the experimentally derived background which in the absence of experimental base line would be the free-atom photoelectric cross section μ_0. As indicated in eq 1, the EXAFS modulation, χ, is not expressed as a function of the incident X-ray photon energy but as a function of the resultant photoelectron wave vector defined by

$$\boldsymbol{k} = 2\pi(2m_e(E - E_0))^{1/2}/h \quad (2)$$

where $\boldsymbol{k}$ is the photoelectron wave vector in ängstroms^{-1}, E is the energy of the incident photon in eV, E_0 is the K-shell binding energy in eV, m_e is the mass of the electron, and h is Planck's constant.

To obtain $\chi(k)$ from an X-ray spectrum, a number of procedures are utilized. First, a pre-absorption edge background is removed from the spectrum. Then the spectrum is divided by the free-atom photoelectric cross section (Victoreen formula) and a low-frequency background is removed. Since only relative absorption cross sections are treated, it is necessary to normalize the spectrum to obtain an edge height of one. In the final operation, the energy spectrum is expressed as a function of photoelectron wave vector space, hereinafter called k space. In order to make this conversion it is necessary to choose a value for the binding energy, E_0, for the excited K electron. At the present time there is no reasonable a priori method for estimating E_0 so approximate values are used for the first iteration.

The next analysis step is to examine the power spectra of the Fourier transforms of $\chi(k)$ multiplied by different powers of $k(k^n(k))$. As can be seem from the theoretical form for $\chi(k)$[7,8]

$$\chi(k) = \sum_{i=1}^{n_s} \frac{N_i}{kR_i^2} e^{+\theta_i k^2} |f_i(k,\pi)| \sin(2kR_i + \alpha_i(k)) \quad (3)$$

(where n_s = number of scattering shells, N_i = number of atoms in the ith shell, R_i = distance to the ith shell in ångstroms (Å), $f_i(k,\pi)$ = backscattering amplitude for the ith shell, σ_i = disorder parameter for the ith shell, and $\alpha_i(k)$ = scattering phase shift). The Fourier transform of the k-space data yields a radial distribution function of the neighboring atoms, hereafter called R space. However, the Fourier transforms give only approximate distances and tentative elemental identifications, due to nonlinearities in the phase shift functions $\alpha_i(k)$ and asymmetry of the amplitude functions $f_i(k,\pi)$. More determinations are made by curve fitting.

The Teo–Lee (T–L) model[9] and the Hodgson–Doniach (H–D) model[19] were used in curve fitting. In the Teo–Lee model, theoretical cal-

(3) Wydrzynski, T.; Marks, T.; Schmidt, P. G.; Govindjee; Gutowsky, H. S. *Biochemistry* **1978**, *17*, 2155.
(4) Blankenship, R. E.; Sauer, K. *Biochem. Biophys. Acta* **1974**, *357*, 152.
(5) Wydrzynski, T.; Sauer, K. *Biochim. Biophys. Acta* **1980**, *589*, 56.
(6) Kirby, J. A.; Goodin, D.; Wydrzynski, T.; Robertson, A. S.; Klein, M. P. *J. Am. Chem. Soc.*, following paper.
(7) Stern, E. A. *Phys. Rev. B.* **1974**, *10*, 3027.
(8) Ashley, C. A.; Donlach, S. *Phys. Rev. B.* **1975**, *11*, 1279.
(9) Teo, B.-K.; Lee, P. A. *J. Am. Chem. Soc.* **1979**, *101*, 2815.
(10) Cramer, S. P.; Hodgson, K. O.; Stiefel, E. I.; Newton, W. E. *J. Am. Chem. Soc.* **1978**, *100*, 2748.
(11) Plaksin, P. M.; Stoufer, R. C.; Mathew, M.; Palenik, G. J. *J. Am. Chem. Soc.* **1972**, *94*, 2121.
(12) Cooper, S. R.; Calvin, M. *J. Am. Chem. Soc.* **1977**, *99*, 6623.
(13) Nyholm, R. S.; Turco, A. *Chem. Ind. (London)* **1960**, 74.
(14) Kincaid, B. M. Ph.D. Thesis, Stanford University, Stanford, CA, 1975.
(15) Jaklevic, J.; Kirby, J. A.; Klein, M. P.; Robertson, A. S.; Brown, G. S.; Eisenberger, P. *Solid State Commun.* **1977**, *23*, 679–682.
(16) Goulding, F. S.; Pehl, R. H. In "Nuclear Spectroscopy and Reactions, Part A"; Academic Press: New York, 1974; p 289.
(17) Hastings, J. B.; Kincaid, B. M.; Eisenberger, P. *Nucl. Instrum. Methods* **1978**, *152*, 167.
(18) (a) Kirby, J. A.; Robertson, A. S.; Klein, M. P., manuscript in preparation. (b) Kirby, J. A. Ph.D. Thesis, University of California, Berkeley, CA, 1980; (c) Smith, J. P. Ph.D. Thesis, University of California, Berkeley, CA, 1978; (d) Robertson, A. S. Ph.D. thesis, University of California, 1979.

culations are used for $f_i(k,\pi)$ and $\alpha_i(k)$ in eq 3 and the values of N_i, α_i, R_i, and E_{0i} are simulataneously fit.[18] In the H-D model, simple functional forms for $f_i(k,\pi)$ and $\alpha_i(k)$ are assumed, and experimental data on model compounds are used to determine them for particular absorber–backscatter pairs.[19]

Each model has its own merits and limitations.[18] In general, the T-L model has the ability to give reasonable fits with highly disordered and chemically altered systems; for certain types of multishell fits, there are too many parameters. The H-D model, on the other hand, has the advantage of simplicity and fewer fitting parameters (only N_i and R_i); it generally gives unreliable values for the number of scatters and poorer fits.[18] In the following discussion, the H-D fits will be included in the tables of results for comparison but in general will not be discussed.

Thus, the general analysis procedure is to perform the Fourier transforms and make estimates of the radial distances and guesses for elements contributing to a given R-space feature. These values and guesses are then used as the starting points in the curve fitting.

The first curve fits performed are on resolved peaks in the R-space Fourier transforms. These fits are used to make elemental identifications and the first determination of the true radial distance to the atoms represented by the peak. The resolved peak is isolated by applying a window function, and this feature is then transformed back to k space for fitting. A number of single-shell fits are performed, using the parameters for several reasonable choices of backscattering elements. With use of the criteria explained in ref 18, the elemental identifications and radial distance determinations are made. If two or more R-space peaks are very close together, it is not possible to accurately use the single-peak and compute multishell fits to make reasonable identification of the ligands involved and their distances. It is often very useful to create simulated data and compare the Fourier transforms and fitting results with the unknown system. The simulated data are essentially equivalent to creating model compounds of known structure. These often aid in identification of complex multidistance R-space peaks.

The last analysis step is to perform multishell fits on a Fourier isolated k-space spectrum which includes all the R-space peaks of interest. This isolation step is only used to remove the residual low-frequency background and high-frequency noise, thereby greatly improving the precision of the fits.

If a single peak can be isolated, there is one additional method that can be used. With single peaks it is possible to remove the amplitude from the spectrum, leaving only a nonlinearily phase modulated sine wave. This permits phase-only T-L fits, which often result in better distance determinations than do total fits.[18] These phase-only fits also provide a method of obtaining distance error estimates.[18] All the single-shell phase-only fits that were performed can be identified in the tables by the presence of error estimates.

Results

Some the of R-space Fourier transform power spectra for the samples studied are presented in Figure 1 and the relative magnitudes and positions for the main peaks are tabulated in Table I. The representations $k^0\chi(k)$ and $k^3\chi(k)$ indicate that $\chi(k)$ was multiplied by k^0 (=1) and k^3, respectively, before the Fourier transform was performed. The purpose in examining the different $k^n\chi(k)$ transforms is to make tentative elemental identifications. With the exception of highly disordered shells, the heavier the element, the higher its relative Fourier transform peak becomes as the power of k^n increases.[18]

Di-μ-oxo-Bridged Manganese Dimers. The $k^0\chi(k)$ and $k^3\chi(k)$ R-space Fourier transforms for Mn(3,4)bpy are presented in Figures 1a and 1b, and the crystal structure is presented in Figure 2. The Fourier transforms for the other two model compounds, Mn(3,4)phen and Mn(4,4)phen, are quite similar so that comparisons of the distances in Mn(3,4)phen and Mn(4,4)phen to the known distances in Mn(3,4)bpy will be made with curve fits.

The curve-fitting results are presented in Table II. Examination of the contents of Figures 1a and 1b and of Table II leads to three immediate observations. First, the actual error for the average distance for the bridge oxygens (0.007 Å) is well within the estimated error (0.019 Å) for the T-L model, so the comparative results for this shell should be quite accurate. Second, the Mn shell is about 0.039 Å shorter than the crystal structure distance, but all three Mn results are short of the crystallographic result of approximately 2.72 Å. This shortening of the Mn–Mn distance seems to be associated with the di-μ-oxo configuration since the only other model compounds examined which had short Mn–Mn distances were Mn_2O_3 and α-MnO_2, which are also di-μ-oxo bridged. Their distances were short by almost exactly the same amount.[18] Thus, all consideration of bridged Mn–Mn distances must take this shortening into account.

The final observation is, perhaps, the most obvious one but at the same time the most perplexing. There is no feature corresponding to the four nitrogens in the first coordination sphere. The large heterogeneity in ligand distances may result in a large interference effect which reduces the nitrogen peak to the noise level. This conclusion was verified by creating a number of different simulations of the oxygen and nitrogen atoms in the first shell of Mn(3,4)bpy (for an example, see Figures 1i and 1j. The effect will be explained in more detail in the Discussion section.

Chloroplasts. The final coadded spectra for the two chloroplast samples represent approximately 200 s of data acquisition per point. The added spectra are presented in Figure 3.

The reduced counting rate for the "shocked" or inactive chloroplast sample is about that expected if two-thirds of the total Mn is released by the Tris treatment and removed by the osmotic shock. (The two samples were similar but not identical in chlorophyll concentration, and the samples were run under slightly different experimental conditions).

Two other experimental effects should be noted. First, due to the much poorer energy resolution on the focused line (>10 eV), the added spectra could not be energy referenced to better than a few electron volts. This results in a small additional dampening effect on the EXAFS modulations. Second, it should be noted that although the EXAFS data extend to higher photon energies, the presence of the iron K edge at 7100 eV forces truncation of the usable EXAFS data at that energy (see Figure 3a).

The first step in analyzing the chloroplast spectra was to examine the Fourier transforms to obtain estimates of ligand distances. By comparison with model compounds and by utilization of the known structural chemistry of Mn, reasonable guesses can be made regarding ligand identity. It should be noted at this point that differentiation between ligands with similar atomic number is not possible with EXAFS at the present time. Therefore, when a reasonable low atomic number ligand of Mn is specified, it will be indicated by CNO representing carbon, nitrogen, oxygen, or some mixture. These elements are all known to ligate Mn, and their dominant presence in chloroplasts strongly suggests them as the most likely ligands of low atomic number. In a similar manner, the next heavier elements likely to be encountered in chloroplasts are indicated by PClS (P, Cl, S) and MnFe (note: Cu cannot be excluded when Mn or Fe is indicated).

a. "Active" Chloroplasts. Fourier transform power spectra for $k^0\chi(k)$ and $k^3\chi(k)$ of the "active" chloroplast spectrum of Figure 3a are presented in Figures 1c and 1d and tabulated in Table I. Examination of Figure 1 and Table I leads immediately to a comparison between (a) the first peak in the active chloroplasts and the oxygen shell in Mn(3,4)bpy (both R_{eff} are approximately 1.3 Å in the $k^3\chi(k)$ transforms) and (b) the third peak of the active chloroplasts and the Mn shell of Mn(3,4)bpy (both R_{eff} are approximately 2.3 Å in the $k^3\chi(k)$ transforms; both grew out of the noise as n in k^n was increased). This similarity is even more striking when the unusual Mn ligand distances represented by these two peaks are compared with other Mn model compounds.[18] Thus, a good starting point was to assume a CNO first coordination sphere ligand at 1.8 Å and a MnFe ligand at 2.7 Å, the crystallographic distances for Mn(3,4)bpy (see Figure 2). The fitting analyses problems, however, were complicated by the presence of the second peak in the transform of the active chloroplast. It was too close to the first peak to be isolated, so all fits on the first two peaks had to perform on the Fourier isolate of these two peaks together. However, the relatively short distance of the second peak (approximately 2.2 Å) and the known chemistry of Mn again suggested CNO ligands.[6,18]

The next step in fitting the active chloroplast spectrum was to examine the isolated third peak in the Fourier transform. With use of the criteria developed for elemental identification (positive

(19) Cramer, S. P.; Eccles, T. K.; Kutzler, F.; Hodgson, K. O.; Doniach, S. *J. Am. Chem. Soc.* **1976**, *98*, 8059.

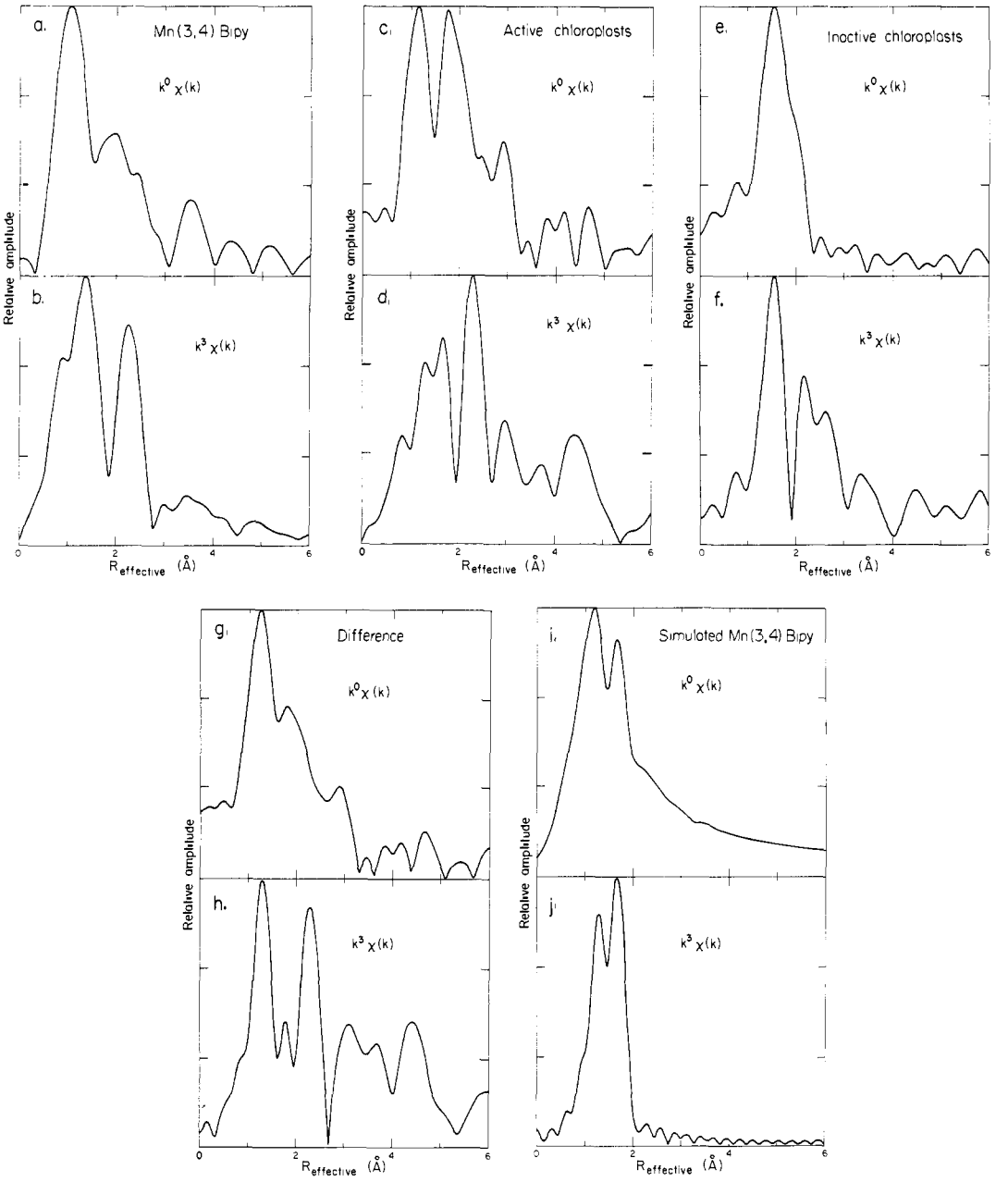

Figure 1. Fourier transforms (power spectra) for a number of different samples with results tabulated in Table I. Spectra a, c, e, g, and i are transforms of $k^0\chi(k)$. Spectra b, d, f, h, and j are transforms of $k^3\chi(k)$. Samples are: (a and b) Mn(3,4)bpy, (c and d) active chloroplasts, (e and f) inactive chloroplasts, (g and h) chloroplast difference, and (i and j) simulated first coordination sphere of Mn(3,4)bpy (see Table I).

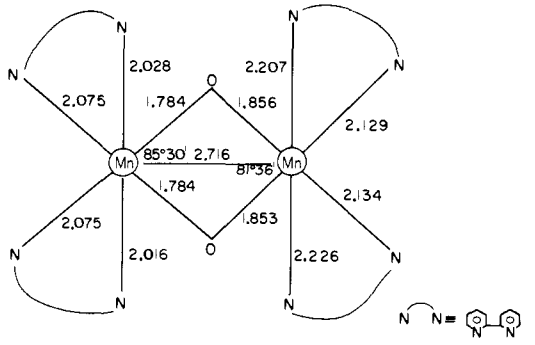

Figure 2. Structure of Mn(3,4)bpy as determined by Plaksin et al.[11]

amplitude at expected distance and comparison of the quality of the fit with different elements),[18,19,21] both fitting models predicted a MnFe atom at an approximate distance of 2.7 Å. Due to the high noise level in the spectrum and the lack of a good separation between the peaks, the reported fitting results for this peak are deferred until consideration of the final three shell fits.

The first two peaks were difficult to identify positively. This was finally accomplished by comparing the Fourier isolation of the first two peaks and some of the simulated Mn(3,4)bpy oxygen–nitrogen first coordination sphere models mentioned earlier. One of the simulations which closely resembled the EXAFS of the active chloroplasts is described in Tables I and III and its Fourier transforms are presented in Figure 1i and 1j. With this valuable clue, it was possible to obtain very good fits to the first two peaks of the active chloroplasts. The isolated spectrum, the simulated spectra, and their best T–L fits are presented in Figure 4. The one- and two-shell fitting results for the isolated and the simulated spectra are tabulated in Table III.

The three-shell fits (using two CNO first shells and a Mn third shell as indicated above) are tabulated in Table IV. The noise-filtered $k^3(k)$ spectrum and its best T–L fit are presented in Figure 5.

b. Inactive Chloroplasts. Analysis of the "inactive" chloroplast spectrum was performed with the primary concern of determining the exact extent to which this spectrum, which represents the

Table I. Fourier Transform (Power Spectra) Peak Positions and Relative Amplitudes (E_0 = 6565 eV)

sample (k-space domain)	peak	$k^0\chi(k)^a$ effective distance, Å	$k^0\chi(k)^a$ rel amplitude	$k^3\chi(k)^a$ effective distance, Å	$k^3\chi(k)^a$ rel amplitude
Mn(3,4)bpy (2.5–13.5 Å^{-1})	O	1.06	1.00	1.37	1.00
	Mn	1.96	0.53	2.26	0.82
active chloroplasts (2.5–12 Å^{-1})	first	1.18	0.48	1.32	0.28
	second	1.79	0.47	1.68	0.32
	third	*c*	*c*	2.30	0.42
inactive chloroplasts (2.5–12 Å^{-1})	first	1.56	1.03	1.57	0.62
	second	*c*	*c*	2.19	0.39
	third	2.53	0.15	2.64	0.31
chloroplast[b] difference (2.5–12 Å^{-1})	first	1.26	0.66	1.31	0.36
	second	1.81	0.42	1.78	0.17
	third	*c*	*c*	2.29	0.32
simulated[d] Mn(3,4)bpy first shell (2.5–13.5 Å^{-1})	O	1.20	1.10	1.29	0.54
	N	1.68	0.97	1.68	0.63

[a] The EXAFS data were multiplied by $k^0 = 1$ and k^3, respectively, before Fourier transformation. [b] The EXAFS data were created by active − (inactive/3). See text. [c] Missing in this Fourier transform. Due to interference effects and noise in the data. Refer to Figure 1a. [d] First-shell simulation constructed by using two O atoms at 1.8 Å, two N at 2.0 Å, and two N at 2.2 Å with $\sigma = -0.001$ for all and the Teo-Lee Model.[9] Amplitude corrected for σ.[18]

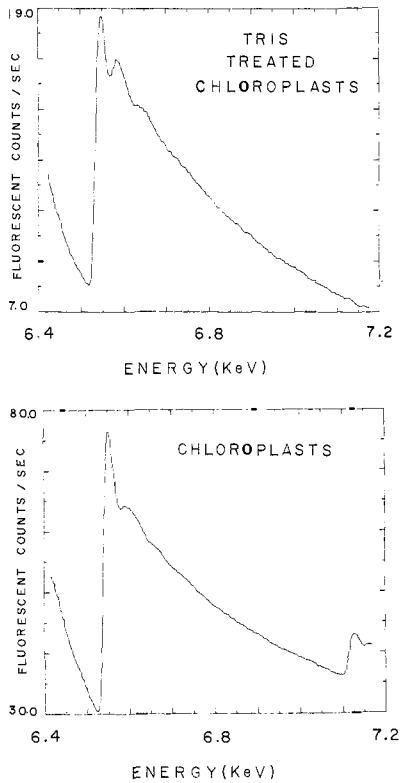

Figure 3. Fluorescence detected X-ray absorption spectra of the Mn k edge for (top) "active" chloroplasts and (bottom) Tris-washed, osmotically shocked or "inactive" chloroplasts.

residual Mn content of chloroplasts after the "loosely bound" Mn was removed, contributes to the "active" chloroplast spectrum. If no evidence of alteration in the state of this "tightly bound" Mn could be found, then an attempt to obtain the (k) spectrum of only the "loosely bound" Mn would be made.

The "inactive" chloroplast Fourier transform power spectra are presented in Figures 1e and 1f, with the peak magnitudes and positions included in Table I. Examination of the inactive chloroplast transforms shows no apparent correspondence between its first peak and those of any of the active chloroplast peaks. Rather, the peak corresponds to a low valent Mn^{2+} to CNO first coordination sphere distance (approximately 2.1 Å when corrected by adding 0.5 Å to the $k^3\chi(k)$ results). The second peak of the inactive chloroplasts, however, seems to lie at approximatey the same distance as the third active chloroplast peak and may thus contribute to the active chloroplast's third peak. The third inactive chloroplast peak, when the high noise level of the spectra is considered, seems to be compatible with being a normal second coordination sphere ligand (approximately 3.1 Å).

Curve fitting on the inactive chloroplasts was not very successful, and as a consequence, only the T–L one-shell fitting results on Fourier isolated R-space peaks are presented in Table V. The first-peak fits show that the ligands observed are definitely CNO-type, but the value obtained for E_0 was 10 eV lower than any other CNO ligand studied, which explains the failure of the H–D model fits.[18] This unusual result may imply that the first

Table II. One-Shell Fits to Isolated Peaks in Mn(3,4)bpy,[a] Mn(3,4)phen,[b] and Mn(4,4)phen[c] (All Fits Were Performed over a Range of k = 4–12 Å^{-1})

	Teo-Lee model				
sample	fitting[i] error	distance[d]	no. of atoms[e]	σ	E_0
Mn(3,4)bpy					
O	0.193	1.812 (19)[g]	1.8	−0.0051	6575.0
Mn	0.016	2.677 (16)[h]	0.9	−0.0068	6548.6
Mn(3,4)phen					
O	0.400	1.811 (19)	2.0	−0.0057	6575.9
Mn	0.034	2.660 (21)[h]	1.2	−0.0105	6544.6
Mn(4,4)phen					
O	0.105	1.778 (16)[g]	1.9	−0.0010	6566.1
Mn	0.014	2.678 (8)[h]	1.0	−0.0069	6546.5

	Hodgson-Doniach model[18,20]			
sample	fitting error	distance	no. of atoms	E_0
Mn(3,4)bpy				
O	0.480	1.790	5.1	6565
Mn	stnd[f]	2.684[f]	1	6565
Mn(3,4)phen				
O	0.650	1.786	6.0	6565
Mn	0.060	2.675	1.2	6565
Mn(4,4)phen				
O	0.038	1.786	4.7	6565
Mn	0.016	2.686	1.0	6565

[a] Di-μ-oxo-tetrakis(2,2'-bipyridine)dimanganese(III,IV) perchlorate. [b] Di-μ-oxo-tetrakis(1,10-phenanthroline)dimanganese-(III,IV) perchlorate. [c] Di-μ-oxo-tetrakis(1,10-phenanthroline)-dimanganese(IV,IV) perchlorate. [d] Phase-only fits, amplitude removed from Fourier isolated peak.[18] [e] Corrected for σ. [f] This Mn was used as the backscattering model with the distance correct for Mn_4N. [g] Mn(3,4)bpy average distance = 1.819 Å. Mn(IV)-O distance = 1.784 Å.[11] [h] Mn(3,4)bpy Mn–Mn distance = 2.716 Å. This distance error of −0.039 Å is characteristic of all di-μ-oxo Mn–Mn distance studies (these compounds and Mn_2O_3).[18] Thus Mn(3,4)phen Mn–Mn = 2.699 Å and Mn(4,4)phen Mn–Mn = 2.717 Å. [i] Average least-square error weighted by k^3.

Table III. Fits on Active Chloroplast Isolated First and Second Shells and Simulated O–N Shell of Mn(3,4)bpy,[a] Using Teo–Lee Model[d] (All Fits Were Performed over a Range of $k = 4$–11 Å^{-1})

sample	fitting atom	fitting error	distance	no.[b] of atoms	σ	ΔE_0[c]
			a. One-Shell Fits			
active	(1) C	0.043	1.830 (48)	1.1	0.0105	−17.7
(1–2)	(2) N	0.049	1.816 (50)	0.8	0.0116	−14.0
	(3) O	0.050	1.802 (52)	0.6	0.0127	−10.3
simulation	(1) C	0.030	1.813 (80)	1.8	0.0097	−18.0
	(2) N	0.031	1.800 (80)	1.3	0.0105	−14.0
	(3) O	0.032	1.786 (80)	1.1	0.0113	−10.3
			b. Two-Shell Fits			
active	(1) O	0.0011	1.791	0.9	0.0068	−8.9
(1–2)	N		2.193	0.4[b]	−0.0104	−3.0
	(2) N	0.0012	1.798	0.8	0.0081	−19.4
	O		2.193	0.4	−0.0027	1.1
simulation	(1) O	0.0002	1.803	1.6	0.0006	−3.9
	N		2.135	1.0[b]	−0.0101	5.3
	(2) N	0.0014	1.802	1.7	0.0020	−12.6
	O		2.143	1.7	−0.0037	12.6

[a] Simulation parameters: two atoms of O at 1.80 Å, two atoms of N at 2.00 Å, two atoms of N at 2.20 Å, all σ_i equal to −0.001. Amplitudes corrected for σ.[18] [b] Corrected for σ. $\sigma < -0.008$ for CNO left uncorrected.[18] [c] For active chloroplasts, difference between best fit E_0 and 6571.2 eV. For simulated file this is the best fit ΔE_0. [d] See ref 9.

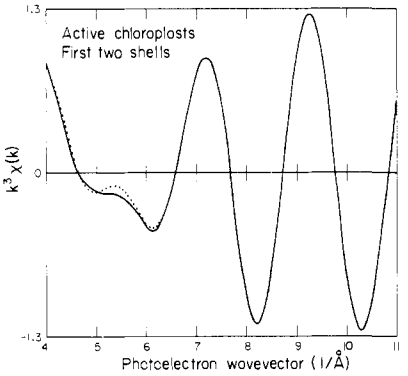

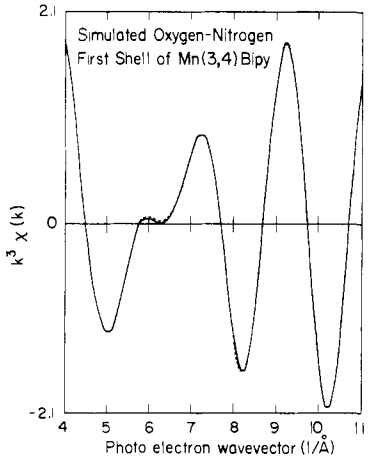

Figure 4. (top) $k^3\chi(k)$ EXAFS spectrum of isolated first two Fourier transform peaks of the "active" chloroplasts (see Figure 1) and the best Teo–Lee[9] two-shell fit, using oxygen and nitrogen ligand atoms. Dotted line is the data and the solid line is the fit. (bottom) $k^3\chi(k)$ simulated EXAFS spectrum of oxygen–nitrogen first coordination sphere of Mn(3,4)bpy corresponding to Figure 1j, whose parameters are described in Tables I and III (dotted line). Solid line is best Teo–Lee two-shell fit, using oxygen and nitrogen ligand atoms.

shell is highly disordered, a hypothesis which could only be explored with significantly better data. The distance observed is approximately 2.1 Å, which suggests that it could be contributing

Table IV. Active Chloroplast Three-Shell Fits (All Fits Were Performed over a Range of $k = 4$–11 Å^{-1})

fitting atoms	fitting error	distance	no. of atoms[a]	σ	E_0
		Teo–Lee model[9]			
(1) O	0.0013	1.851	1.4	−0.0073	6569.3
N		2.046	3.3[b]	−0.0195	6549.1
Mn		2.703	0.44	−0.0049	6553.4
(2) N	0.0036	1.789	1.0	0.0065	6549.2
O		2.207	0.6	0.0144	6582.0
Mn		2.688	0.45	−0.0040	6550.7
		Hodgson–Doniach model[18,20] ($E_0 = 6565$ eV)			
(1) O	0.0460	1.843	2.72		
N		2.133	1.38		
Mn		2.690	0.55		
(2) N	0.0490	1.871	1.21		
O		2.135	3.41		
Mn		2.686	0.55		

[a] Corrected for σ.[18] [b] $\sigma < -0.008$ for CNO left uncorrected.[18]

Table V. Inactive Chloroplast Fits Using One Shell (All Fits Were Performed over a Range of $k = 4$–11 Å^{-1})

fit no.	fitting atom	fitting error	distance[a]	no. of atoms[b]	σ	E_0
			Teo–Lee Model[9]			
			a. Isolated First-Peak Fits			
1	C	0.157	2.106 (44)	2.5	−0.0059	6546.2
2	N	0.124	2.085 (36)	2.1	−0.0048	6548.7
3	O	0.094	2.068 (31)	1.8	−0.0039	6550.7
			b. Isolated Second-Peak Fits			
1	C	0.0196	2.716 (24)	3.3	0.0008	6548.2
2	N	0.0128	2.696 (18)	2.6	0.0019	6550.0
3	O	0.0079	2.677 (12)	2.1	0.0027	6551.8
4	S	0.0195	2.676 (10)	−1.2	−0.0034	6551.3
5	Mn	0.0507	2.674 (8)	0.44	−0.0099	6540.7

[a] Phase-only fits.[18] [b] Corrected for σ. for sulfur, a multiple Mn amplitude correction was used.[18]

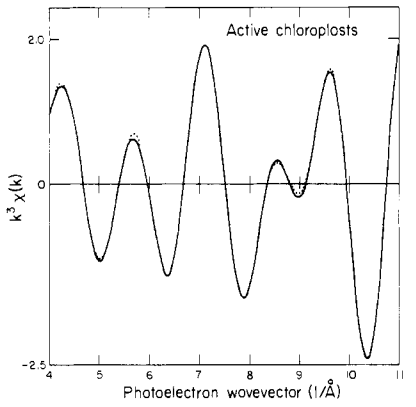

Figure 5. $k^3\chi(k)$ spectrum for the three main Fourier transform peaks of the "active" chloroplasts (see Figure 1d) and the best Teo–Lee[9] three-shell fit (using oxygen, nitrogen, and manganese ligand atoms, respectively). The dotted line is the data and the solid line is the fit.

to the active chloroplast's second peak. The second and third peaks in the inactive chloroplast power spectrum could not be separated by the Fourier isolation technique, and no acceptable two-shell fits were obtained. It was necessary to examine the second peak to see if it might be contributing to the third peak in the active chloroplast power spectrum. A Fourier isolation was performed, and the one-shell fitting results are included in Table V. With use of the criteria developed to approximately identify the element

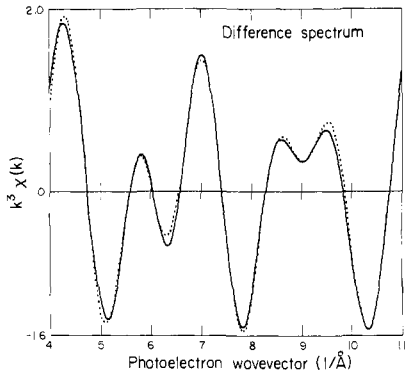

Figure 6. $k^3\chi(k)$ difference spectrum of "active" chloroplast spectrum minus "inactive" chloroplast spectrum divided by 3 and the best Teo-Lee[9] three-shell fit (using oxygen, nitrogen, and manganese ligand atoms, respectively). The dotted line is the difference and the solid line is the fit.

of a transform peak, the one-shell results indicate MnFe based on the qualitative features of the fit. In any case, it has the right distance to be present as part of the active chloroplast's third peak and thus could represent about one-third of the magnitude of that peak.

From this analysis it appears that the "tightly bound pool" of Mn did not appear to be affected by removing the "loosely bound pool" of Mn. Thus, if the inactive chloroplast spectrum is multiplied by one-third and subtracted from the active chloroplast spectrum, the difference should be a reasonable representation of the EXAFS of the "loosely bound" Mn. The resulting Fourier transforms are presented in Figures 1g and 1h and Table I.

c. Difference Spectrum. Examination of the transforms of this "difference" spectrum created to simulate the EXAFS spectrum for the "loosely bound pool" of Mn shows a marked reduction and slight position shift in the second peak and a 25% reduction in magnitude for the third peak when compared to the peaks of the active chloroplasts. This is exactly the result expected from comparing the transform peak magnitude of the active and inactive chloroplasts and then forming the difference in R space.

The curve fits were then performed in a similar manner as before with the same ligand shells as previously identified for the active chloroplasts. The results are listed in Table VI, and the difference spectrum and its best fit are presented in Figure 6.

Discussion

Di-μ-oxo Manganese Dimers. Examination of Table II reveals a very interesting structural result. The bridging oxygens have the same average distance in Mn(3,4)bpy and Mn(3,4)phen, while the oxygens in Mn(4,4)phen have the same average distance as the Mn(IV)–oxygen distance in Mn(3,4)bpy. The Mn–Mn distances for Mn(3,4)bpy and Mn(4,4)phen are the same, while the Mn(3,4)phen Mn–Mn distance is 0.02 Å shorter. These results thus predict changes in the Mn_1–O–Mn_2 bond angles. Using the average distances from Table II and assuming the same ligand distance difference as in Figure 2, the Mn_1–O–Mn_2 angles would be (1) 96.5° for Mn(3,4)bpy (from the crystal structure[11]), (2) 93.9° for Mn(3,4)phen, and (3) 97.7° for Mn(4,4)phen. These are obviously not very large angular changes and therefore would seem to be quite reasonable results. Should the crystal structures of Mn(3,4)phen and Mn(4,4)phen be obtained in the future, they will provide very good additional tests of the ability of EXAFS to measure small differences in structurally similar systems.

As mentioned earlier, an explanation for the problem of the missing nitrogen shells in Mn(3,4)bpy, Mn(3,4)phen, and Mn(4,4)phen was developed by examining different simulations of the first coordination sphere of Mn(3,4)bpy. The simulations were constructed by using the T–L model values with two oxygen atoms at 1.8 Å, two nitrogen atoms at 2.0 Å, and two nitrogen atoms at 2.2 Å. The values of σ_i (see eq 3) were than varied to model variable amounts of static and thermal disorder. The simulations had two surprising results. First, if the σ_i's were equivalent and small, the result was one nitrogen transform peak, not two as expected, and it was not twice as large as the oxygen peak. One example of this result is given in Figures 1i and 1j with its numerical analysis tabulated in Table I. This implies that the nitrogen shells were strongly interfering and while perturbing the oxygen shell transform peak, the strongest effect was upon their own transform peak. Second, if the σ_i's for the nitrogen atoms were signifiicantly more negative than for the oxygen peak (for example, $\sigma_N = -0.005$ and $\sigma_O = -0.001$), then the nitrogen atoms badly interfere, resulting in a very small transform peak which would be masked in the model compound transforms by the presence of the Mn peak and a finite noise level. The crystal structure of Mn(3,4)bpy (Figure 2) shows that the nitrogen atoms are significantly more disordered than are the oxygen atoms[11] so the disappearance of the nitrogen transform peak is not an unphysical result.[20]

A final question which requires consideration concerns the validity the di-μ-oxo manganese dimers as general model compounds for CNO-bridged transition-metal dimers, since their analyses are cornerstones in the analysis of the active chloroplast "loosely bound pool" of Mn. An extreme change that could be made would be to reduce the Mn atoms[6] and substitute carbon, a much "softer" ligand, for the nitrogen and bridging oxygen ligands. A number of Mn(II) dimer systems with all carbon ligands have been synthesized and studies by Anderson and coworkers.[22] The surprising results are a 2.72 Å Mn–Mn distance

Table VI. Fits on Chloroplast Difference (All Fits Were Performed over a Range of $k = 4$–11 Å^{-1})

fitting atoms	fitting error	distance	no. of atoms	σ	E_0
Teo–Lee model[9]					
		Two-Shell Fits			
(1) O	0.0344	1.791	0.99[a]	0.0035	6550.0
Mn		2.711	0.89[c]	−0.0279	6557.6
(2) N	0.0410	1.806	1.24[a]	0.0025	6546.0
Mn		2.710	0.87[c]	−0.0277	6557.7
		Three-Shell Fits			
(1) O	0.0063	1.812	0.92[a]	0.0073	6557.4
N		2.139	0.32[a]	−0.0026	6583.0
Mn		2.694	0.23[c]	−0.0225	6554.8
(2) N	0.0067	1.809	0.94[a]	0.0101	6548.0
O		2.077	0.43[b]	−0.0563	6583.0
Mn		2.706	0.29[c]	−0.0188	6556.2

fitting atoms	fitting error	distance	no. of atoms
Hodgson–Doniach model[18,20] ($E_0 = 6565$ eV)			
	Two-Shell Fits		
(1) O	0.243	1.865	0.80
Mn		2.682	0.39
(2) N	0.162	1.848	1.85
Mn		2.678	0.39
	Three-Shell Fits		
(1) O	0.0054	1.854	3.10
N		2.111	1.13
Mn		2.677	0.39
(2) N	0.0222	1.888	1.51
O		2.130	2.85
Mn	q	2.676	0.38

[a] Corrected for σ.[18] [b] $\sigma < -0.008$ CNO shell left uncorrected.[18] [c] $\sigma < -0.023$ for single Mn shell left uncorrected.[18] Note that, in general, the larger σ, the smaller the number of atoms predicted by the fit. If the slope for Mn correction from ref 18 is used, then all four numbers of Mn atoms are equivalent ±10%.

(20) Eisenberger, P.; Brown, G. S. *Solid State Commun.* **1979**, *29*, 481.
(21) (a) Cramer, S. P.; Hodgson, K. O.; Stiefel, E. I.; Newton, W. E. *J. Am. Chem. Soc.* **1978**, *100*, 2748; (b) Cramer, S. P.; Hodgson, K. O.; Gillum, W. O.; Mortenson, L. E. *Ibid.* **1978**, *100*, 3398; (c) Cramer, S. P.; Gillum, W. O.; Hodgson, K. O.; Mortenson, L. E.; Stiefel, E. I.; Chisnell, J. R.; Brill, W. J.; Shah, V. K. *Ibid.* **1978**, *100*, 3814.

Table I. Interacting Bands (x), Main CD Characteristics Obtained by DeVoe Treatment (Lines 1–9) in Set a Computations, and Experimental Values (Line 10)

	bands						Δε			
line	benzenoid 4.30 μm⁻¹ (233 nm)	quinoid 3.64 μm⁻¹ (275 nm)	dienic 4.44 μm⁻¹ (218 nm)	dienonic 3.91 μm⁻¹ (256 nm)	amidic 5.2 μm⁻¹ (193 nm)	olefinic 5.2 μm⁻¹ (193 nm)	3.6 μm⁻¹	3.9 μm⁻¹	4.2 μm⁻¹	4.8 μm⁻¹
1	x				x				−0.02	−0.03
2	x					x		0.4	−2.8	−4.4
3	x		x				0.0	1.2	28	−19
4	x	x	x				−10	2	37	−18
5		x		x			−17	21	3	0.3
6	x	x	x	x			−20.6	19.2	36.4	−19
7	x	x	x	x		x	−20.8	18	31.4	−24.3
8	x	x	x	x	x	x	−20.7	17.6	34.6	−44.7
9	x	x	x	x	x	x	−16.1	15.3	32.9	−45.3
10	exptl						−24	15	41.5	−54

Table II. Interacting Bands (x) and Main CD Characteristics Obtained in Set b Computations

	bands				Δε			
line	benzenoid 4.30 μm⁻¹ (233 nm)	quinoid 3.64 μm⁻¹ (275 nm)	dienonic 3.91 μm⁻¹ (256 nm)	olefin 5.2 μm⁻¹ (193 nm)	3.6 μm⁻¹	3.9 μm⁻¹	4.2 μm⁻¹	4.8 μm⁻¹
1	x	x	x		−25.3	23.1	7.9	2
2	x	x	x	x	−25.6	22.2	2	−9

Table III. Interacting Bands (x) and Main CD Characteristics Obtained in Set c Computations

	bands					Δε			
line	benzenoid 4.3 μm⁻¹ (233 nm)	quinoid 3.64 μm⁻¹ (275 nm)	diene 4.44 μm⁻¹ (218 nm)	amide 5.2 μm⁻¹ (193 nm)	olefin 5.2 μm⁻¹ (193 nm)	3.6 μm⁻¹	3.9 μm⁻¹	4.2 μm⁻¹	4.8 μm⁻¹
1	x	x	x			−13.8	7.8	37.6	−25
2	x	x	x	x		−13.7	10.6	45.7	−36
3	x	x	x	x	x	−14.3	12	37	−43

account for a more complete treatment because the coupling of these transitions with those of the chromophores considered can affect the higher energy side of the spectrum observed.[24] In addition, static contributions[19] have been completely disregarded owing to the dynamic character of the treatment used.

The main CD characteristics obtained by the DeVoe treatment of calculations in sets a, b, and c are reported in Tables I, II, and III, respectively. Table I contains also the prominent experimental values (line 10).

Taking the results shown in Table I as a reference, we can make the following general comments. The calculations with couples of dipoles (Table I, lines 1–3, 5) show the shape of the experimental CD spectrum can be reproduced only when the quinoid transition at 275 nm interacts with the dienoic one at 256 nm (line 5) and when the benzenoid transition (233 nm) interacts with the diene transition (218 nm) (line 3).

The calculated spectral features of the different partners in the couplet are in complete disagreement (lines 1 and 2) with that experimentaly found (line 10).

The Δε values that more closely approach the experimental ones have been obtained, taking into account four polarizabilities all together (line 6); the introduction of additional polarizabilities does not affect, at least in a relevant extent, the results (line 7 and 8).

The results are qualitatively unaffected also by varying the location of the dienone dipole, and line 9 shows the largest variation observed by changing the dipole location along the diene–amide backbone.

Only the CNDO–SCF–CI polarization directions of the naphtoquinoid transitions[9] give agreement between calculated and experimental CD values.

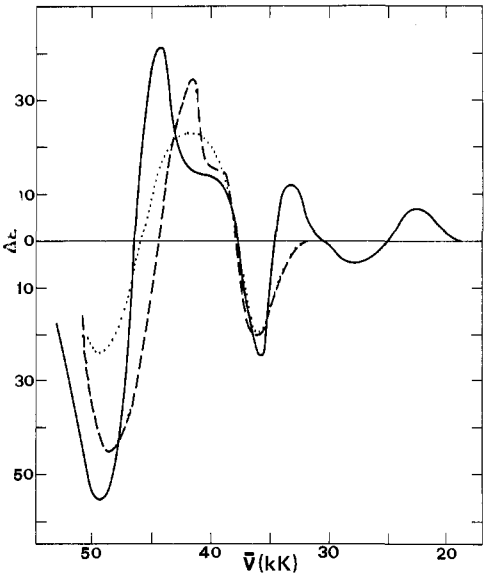

Figure 6. Experimental (–) and calculated [(- - -) set a, (···) sets b and c)] CD spectra of I.

The best calculated CD spectrum is compared with the experimentally detected one in Figure 6.

Tables II and III show the best results obtained when the "dienone" transition at 256 nm and the diene transition at 218 nm interact separately with the two naphthoquinoid absorptions at 275 and 233 nm.

Figure 6 reports the CD spectrum obtained from the weighted average of set b and set c calculations, assuming an equilibrium constant of 1 for the interconversion reaction between the two conformations. The spectrum is compared with the CD spectrum

(24) (a) Zandomeneghi, M. *J. Phys. Chem.* **1979**, *83*, 2926; (b) Drake, A. F.; Mason, S. F. *Tetrahedron* **1977**, *33*, 937; (c) Snyder, P. A.; Johnson, W. C., Jr. *J. Am. Chem. Soc.* **1978**, *100*, 2939.

Table VII. Proposed Ligand Structure of the Photosynthetically Active, "Loosely Bound" Pool of Manganese in Spinach Chloroplasts

ligand[a]	average distance[b]	no.
CNO[c]	1.81 (2)	2–3
CNO	2.15 (5)	2–4
MnFe[c]	2.72 (2)	1

[a] CNO = carbon, nitrogen, or oxygen; MnFe = manganese or iron or copper. [b] Average results for various fits. [c] Bridged structure with CNO ligands and MnFe ligands in approximately square or trigonal bypyrimid arrangement.

the second peak may not be due to bridged Mn atoms but are due to other Mn atoms that are also released during inactivation. If this is the case, then it will be necessary to study the photosynthetically active Mn in its native environment free of contamination of other Mn atoms that may be present and serve other functions. The possibility of multiple sites would also explain the low absolute number of atoms predicted by the fitting results, but at the present time this should be treated as conjecture until some new evidence indicates otherwise.

The change in the ligand ratio is most likely due to the poorer quality of the difference data but should not be totally discounted.

Conclusion

Three di-μ-oxo Mn dimers were examined by using the EXAFS technique. The crystal structure of one of the dimers has been published.[11] Using this published crystal structure, we made determinations concerning certain of the structural parameters for the other two compounds. These results were presented in part a of the Discussion section above.

Part of the study of the Mn dimers was concerned with determining why the nitrogen atoms in the first coordination sphere of the dimers did not appear in the EXAFS spectra. A simulation study showed that large disorder in the Mn–N distances are responsible. This simulation study then led to identification of the first two peaks of the active chloroplast Fourier transforms (see Figure 1).

EXAFS studies on the two chloroplast samples and comparison of the chloroplast results with the bridged Mn dimer models has resulted in a prediction for the local structure of the "loosely bound pool" of Mn in chloroplasts, which is implicitly related to photosynthetic oxygen evolution. The analysis is compatible with a CNO-bridged transition-metal dimer (or multimer) similar to the core of the Mn dimer models studied. The chemistry of Mn suggests that oxygen is the most likely bridging ligand but carbon and nitrogen cannot be excluded. The partner transition metal is most likely another Mn, but Fe and Cu cannot be excluded due to their relative abundance in chloroplasts. The remainder of the first coordination ligands is most likely CNO. The distances for the bridging ligands and the other transition-metal ligands are quite accurately predicted, but the distance for the other first coordination sphere ligands is poorly defined primarily due to a large spread in the individual ligand distances (see Table VII).

Future Work

Obvious extensions now in progress are the effects of actinic light, the effects of various redox reagents and known cofactors such as Cl^-. Most important will be the results obtained from a study of the Mn-containing protein, whose isolation has been only recently reported by Spector and Winget.[24]

Acknowledgment. We thank Dr. T. Wydrzynski, D. Goodin, and A. McGuire for helping to characterize the chloroplast samples used in this study. We thank Professors J. F. Dodge and D. Coucouvanis for gifts of samples, T. Walker, N. Kafka, and A. Ramponi for help in different phases of the data collection at SSRL, and Professor K. Sauer and Dr. B. McQuillan for useful discussions. M.P.K. was the recipient of a Fellowship from the John Simon Guggenheim Foundation during the course of this work and expresses his thanks to the Foundation and to Dr. M. Gueron, Ecole Polytechnique, Palaiseau, and Dr. Y. Farge, L. U.R.E. University of Paris-South. This work was performed under the auspicies of the Divisions of Biomedical and Environmental Research and Basic Energy Sciences of the U.S. Department of Energy under Contract W-7405-ENG-48 and the National Science Foundation under Grant PCM 78-12121. Synchrotron Radiation facilities were provided by the Standford Synchrotron Radiation Laboratory, which is supported by NSF Grant DMR-07692-AO2 and the U. S. Department of Energy.

(23) The "inactive" chloroplast sample of this presentation corresponds to the tris-treated osmoticalloy shocked" or "shocked" chloroplast sample of ref 6.

(24) Spector, M.; Winget, G. D. *Proc. Natl. Acad. Sci. U.S.A.* **1980**, *77*, 957.

State of Manganese in the Photosynthetic Apparatus. 2. X-ray Absorption Edge Studies on Manganese in Photosynthetic Membranes

J. A. Kirby, D. B. Goodin, T. Wydrzynski, A. S. Robertson, and M. P. Klein*

Contribution from the Laboratory of Chemical Biodynamics, Lawrence Berkeley Laboratory, University of California, Berkeley, California 94720. *Received December 1, 1980*

Abstract: X-ray absorption spectra at the manganese K edge are presented for spinach chloroplasts and chloroplasts that were Tris treated and hence unable to evolve oxygen. A significant change in the electronic environment of manganese is observed and is attributed to the release of manganese from the thylakoid membranes with a concomitant change in oxidation state. A correlation of the K-edge energy, defined as the energy at the first inflection point, with coordination charge has been established for a number of manganese compounds of known structure and oxidation state. Comparison of the manganese K-edge energies of the chloroplast samples with the reference compounds places the average oxidation state of the chloroplasts between 2+ and 3+. With use of the edge spectra for Tris-treated membranes which were osmotically shocked to remove the released manganese, difference edge spectra were synthesized to approximate the active pool of manganese. Coordination charge predictions for this fraction are consistent with an average resting oxidation state higher than 2+. The shape at the edge is also indicative of heterogeneity of the manganese site, of low symmetry, or both.

The production of oxygen in photosynthesis by green plants and blue-green algae has been the subject of innumerable studies in the last 50 years. One of the results of these studies has been the demonstration of a manganese requirement for oxygen evolution.[1-3]

0002-7863/81/1503-5537$01.25/0